Proc. Indian Acad. Sci. (Earth Planet. Sci.), Vol. 99, No. 3, September 1990, pp. 425–438.

Entrainment of circumpolar water in the Indian Ocean region of the Antarctic

G S SHARMA* and BENNY N PETER

Cochin University of Science and Technology, School of Marine Sciences, Cochin 682016, India

* Present Address: Marine Science and Fisheries Centre, P.O. Box No. 467, Muscat, Sultanate of Oman

MS received 12 October 1989; revised 27 August 1990

Abstract. The net influx of the circumpolar water on the western (approximately along 10°E) and eastern (approximately 115°E) boundaries of the Indian Ocean, adopting the method of Montgomery and Stroup is computed on bivariate distribution of potential thermosteric anomaly and salinity to identify the characteristics of the flux. The zonal flux at both the boundaries indicates an alternate strong easterly and westerly flow between 36°S and 45°S, south of which the flow is mainly easterly but weak up to 56°S. At the western boundary the easterly flow is 146 Sv and westerly is 98·07 Sv, while at the eastern boundary (115°E) the corresponding fluxes are 123·46 Sv and 27·20 Sv respectively, indicating a net outflux of 48·33 Sv. This water should have been accounted by the melting of ice and influx of the Equatorial Pacific Ocean Water.

Keywords. Entrainment; zonal flux; Antarctica; Indian Ocean.

1. Introduction

For the last few decades the attention of oceanographers has been directed at the Antarctic circumpolar ocean and studies have been made to reveal its structure and transport, as these factors play a major role in the oceanic and atmospheric circulations. Also, as a connecting link between the three major oceans, Antarctic Ocean influences the global distribution of oceanic waters.

The flow of circumpolar water is mainly determined by the eastward flowing Antarctic circumpolar current (figure 1). The Antarctic circumpolar current extends from the Antarctic divergence in the south to the subtropical convergence in the north. The surface flow of the Antarctic circumpolar current is driven primarily by the west wind, the frictional stress combined with the coriolis force giving a northward component. Current meter records coupled with hydrographic observations have demonstrated that the Antarctic circumpolar current is strongly baroclinic.

Computations of mass transport of the circumpolar current have been carried out by Sverdrup *et al* (1942) and Kort (1962). Several transport estimates were done using the data collected in 1975, during ISOS program at Drake passage; $110–138 \times 10^6\ m^3/s$ (Nowlin *et al* 1977), $139 \pm 36 \times 10^6\ m^3/S$ (Bryden and Pillsbury 1977) and $127 \pm 14 \times 10^6\ m^3/s$ (Fandry and Pillsbury 1979). Jacobs and Georgi (1977) estimated the baroclinic geostrophic transport relative to the deepest observations on two meridional sections in the Indian Ocean region of the Antarctic Ocean. The

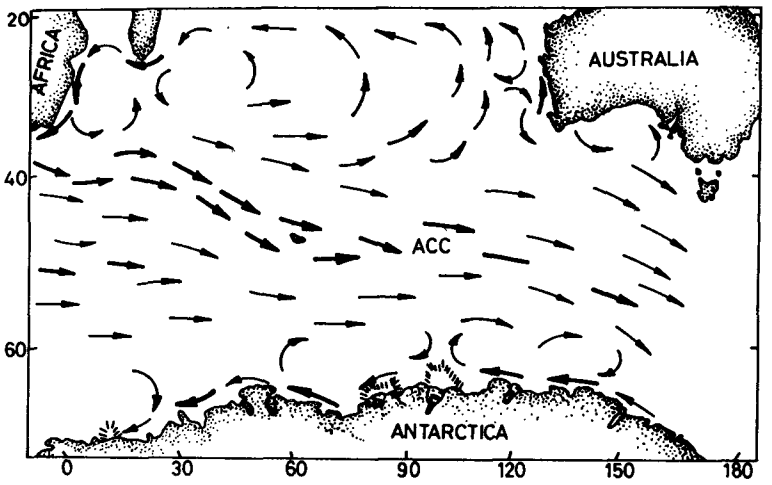

Figure 1. Surface currents in the Indian Ocean region of the Antarctic Ocean during summer.

interoceanic exchanges of heat and freshwater were computed by Georgi and Toole (1982).

The present study aims at obtaining the entrainment of the circumpolar water in the Indian Ocean region off the Antarctica by comparing the zonal fluxes at the western and eastern-most boundaries of the Indian Ocean region of the Antarctic. The western boundary is considered along 10°E while the eastern is 115°E.

2. Materials and methods

The data obtained from the cruises of ARA Islas Orcadas (1976) approximately along 10°E and USNS Eltanin (1970) approximately along 115°E, being covered in summer to avoid seasonal effects, were used to compute zonal fluxes. Since a deep zonal flow is observed (Callahan 1971; Reid and Nowlin 1971; Bryden and Pillsbury 1977) in the Southern Ocean, the mass transport was estimated referring to a level of 3000 db. Hence, the data at hydrographic stations, extending to deeper than 3000 m were only made use of. The geographic distribution of the stations is shown in figure 2.

The zonal flux was estimated by adopting the method introduced by Montgomery and Stroup (1962), using the function of acceleration potential $\phi_a + P\delta$ (Montgomery and Spilhaus (1941) with a modification of using potential temperature instead of the temperature *in situ*.

The acceleration potential is given by

$$\phi_a + P\delta_\theta = P_0\delta_{\theta_0} + \int_{\delta_{\theta_0}}^{\delta_\theta} P\,\mathrm{d}\,\delta_\theta$$

where $\phi_a = \int_P^{P_0} \delta \mathrm{d}P$ the geopotential anomaly relative to the reference pressure. P_0 is the reference pressure and δ_{θ_0}, the potential thermosteric anomaly at the reference pressure. This method can directly lead to the estimation of geostrophic currents at

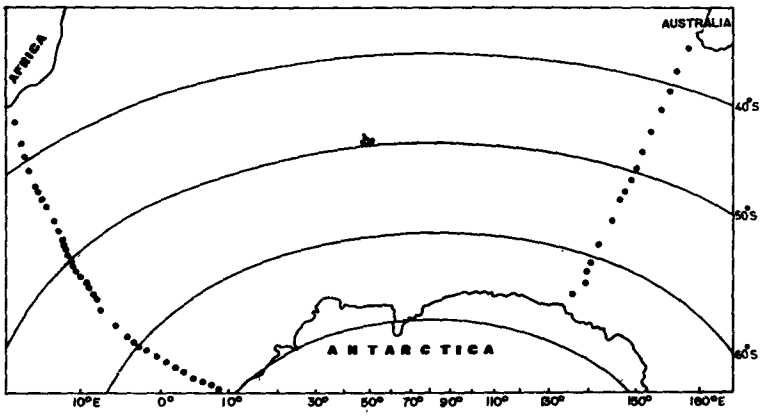

Figure 2. Station positions.

chosen isanosteric surfaces. The zonal component of geostrophic velocity (u) is then calculated from

$$u = \frac{\phi_A - \phi_B}{\left(\frac{f_1 + f_2}{2}\right) L},$$

where ϕ_A and ϕ_B are acceleration potential at stations A and B respectively, L is the distance between the stations and f_1 and f_2 are the coriolis parameters at stations A and B respectively, and Ω is the angular velocity of the earth.

The geostrophic velocity at different isanosteres up to the surface is computed between two stations. From the length and the mean thickness of each quadrangle defined by standard isanosteres and whole degrees of latitude, the mean velocity of the water flowing through it and flux is estimated. The computed geostrophic flux is then divided into each bivariate class defined by potential thermosteric anomaly and salinity using vertical sections, which leads directly to the estimation of geostrophic currents at chosen isanosteric surfaces. This method not only gives the quantitative estimate but also the characteristics of the water flowing. The earlier computations were carried out using the dynamic method and the present method has the advantage that velocities are computed along isanosteric surfaces along which the oceanic flow is assumed to take place.

Eastward (positive) and westward (negative) fluxes are separately displayed for each characteristic interval of 20 cl/t in potential thermosteric anomaly and 0·2‰ in salinity. The total flux between any two consecutive intervals of potential thermosteric anomaly is shown at the bottom and that of salinity on the right hand side of the diagram. In the figures transport values marked by stars and circles are of those classes that together contribute 50% of the total eastward and westward transport and are said to be within the 50% boundary. Since the transport is quite high, the SI system of units is chosen for flux which is million cubic meters per second. In the text, the unit Sverdrup (Sv) is used to denote the fluxes $1\,\text{Sv} = 10^6\,\text{m}^3/\text{s}$. Hereafter, the terms temperature and thermosteric anomaly are used instead of potential temperature and potential thermosteric anomaly.

The geostrophic velocity is computed between two successive stations by choosing 3000 db as the reference level. It is assumed that the reference surface is uniform over the whole meridional extent which may not be correct and slight errors may occur in the estimation of mass transport. Another possible error is that since flux is estimated referring to a deeper level, the potential thermosteric anomaly which is used instead of specific volume anomaly in computing the acceleration potential, may not override the pressure effects completely.

3. Distribution of hydrographic properties

The vertical sections of temperture, salinity and thermosteric anomaly along 10°E and 115°E are presented. Since strong gradients are observed in the upper layers compared to the deeper layers, the depth scale is exaggerated in the upper 500 m. The contours are drawn at different intervals, depending on the gradients, in order to bring out the maximum details possible.

3.1 *Along 10°E*

This section covered during summer extends from the coast of South Africa to the Antarctic Coast (figure 3). The most conspicuous feature is the crowding of isotherms in the northern end where the Agulhas Current and its retroflection occur. The sub-Antarctic front, the northern limit of the polar front zone, is evident at 46°S whereas this zone is limited in the south by the Antarctic polar front at about 50°S. Another interesting phenomenon observed is the presence of the dicothermal layer where the cold water is sandwiched between warm waters above and below. This layer extends from 50°S to Antarctic Coast and lies between 25 and 160 m depths. The cold water is the winter water trapped between warm summer surface layer and the warm deep layer.

During summer along 10°E, the surface water has a salinity range of 33·8–35·5‰ (figure 4). A weak halocline exists below the surface layer between 100 and 200 m. Salinity remains almost constant below the halocline and it is about 34·7‰ in the Antarctic zone at around 500 m depth. The orientation of isohalines at 56° and 64°S in the surface layers suggests the occurrence of upwelling. At the subtropical convergence zone, a salinity variation of 1·0‰ within 1° lat. is observed in the surface. A comparatively strong gradient at 50°S identifies the position of the Antarctic polar front whereas the sub-Antarctic front is at about 46°S. The horizontal salinity gradient is maintained down to the deeper level at the polar front.

The most prominent feature observed in the vertical profile of potential thermosteric anomaly (figure 5) is the strong gradients in the northern part (between 36°S and 43°S), associated with the powerful Agulhas and its return current. The density gradient also indicates that these flows are strong even in the deeper layers. The denser water of the sub-Antarctic and the lighter water from the subtropics seem to meet at the subtropical frontal region, at about 42°S, where intense gradient in density is observed. The orientation of the isanosteres indicates the continuous band of eastward flowing Antarctic circumpolar current between 42° and 54°S. The maximum flow seems to be associated with the polar front at about 50°S. The wavy nature of isanosteres beyond 55°S towards the Antarctic Coast reveals a complex current pattern in this

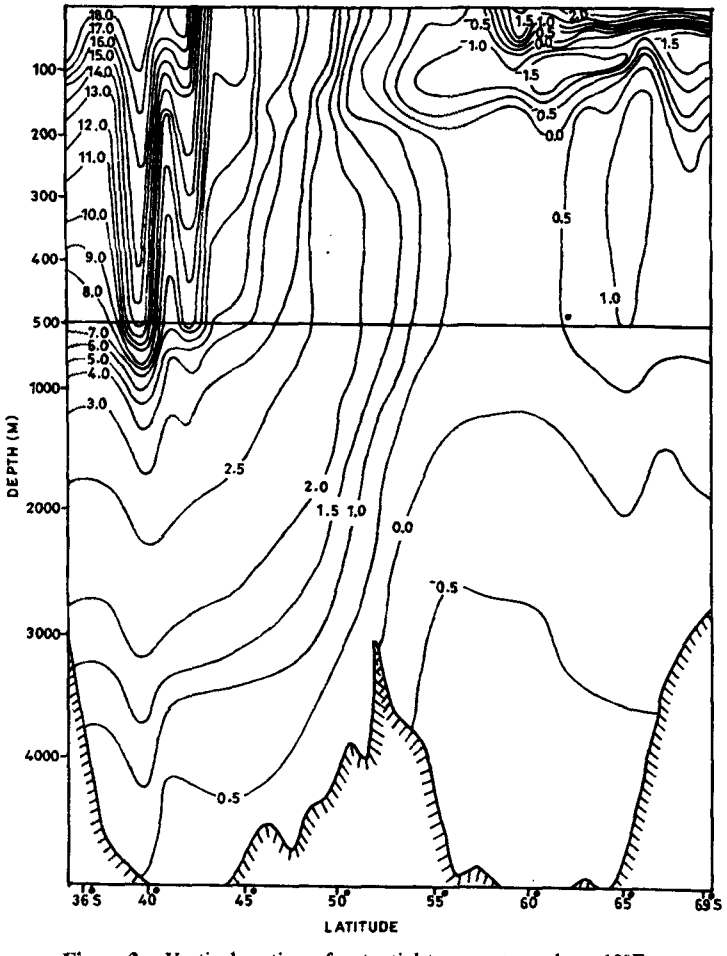

Figure 3. Vertical section of potential temperature along 10°E.

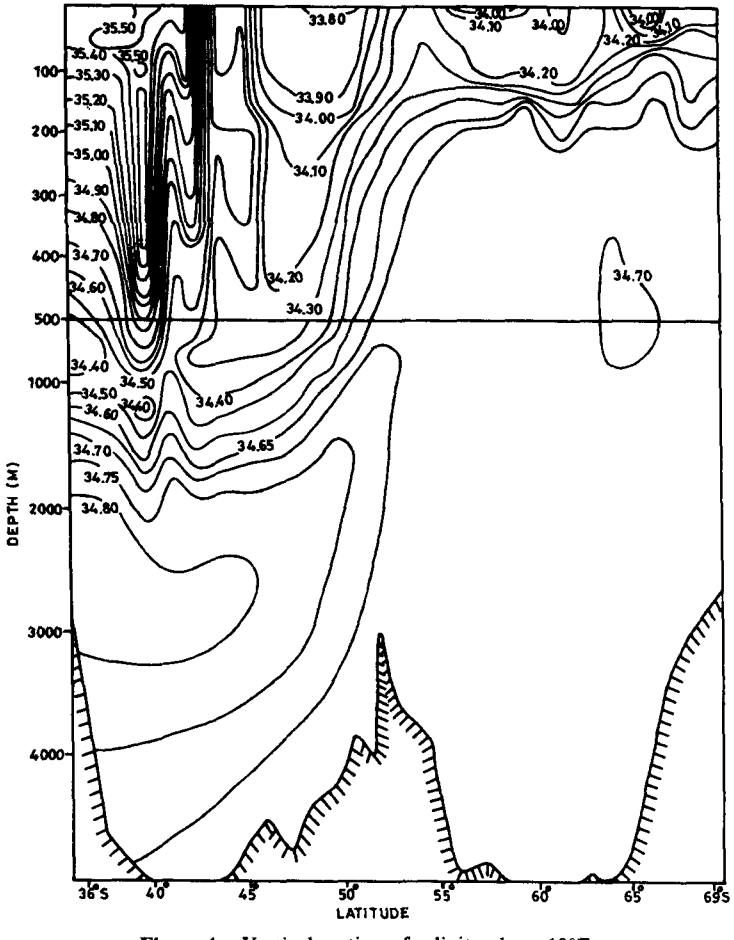

Figure 4. Vertical section of salinity along 10°E.

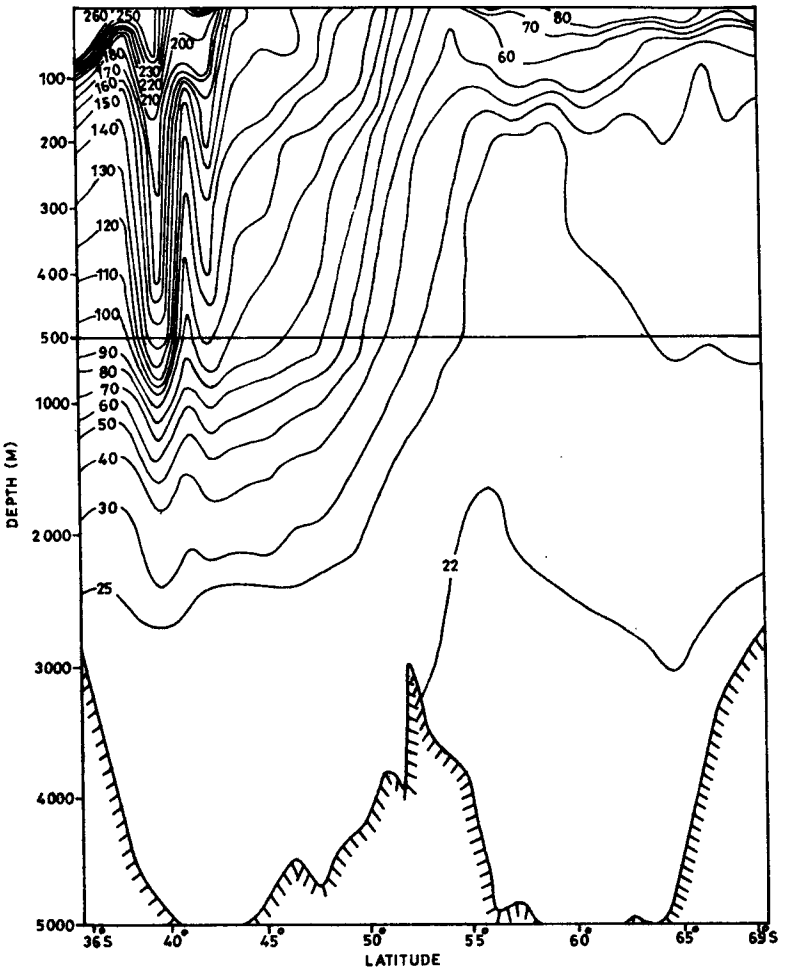

Figure 5. Vertical section of potential thermosteric anomaly along 10°E.

zone. Near the Antarctic Coast, downward sloping of isanosteric surfaces implies a weak westward flow.

3.2 *Along 115°E*

Although this section (36°S–64°S) is covered during summer, the surface of the Antarctic zone records sub-zero temperature (figure 6). The thermocline between 50 and 150 m shows a temperature gradient of 2°C per 100 m. Compared to the western section a large difference of temperature is observed in this section along the same latitude (at 36°S, along 10°E the temperature is 18°C whereas along 115°E it is only 12°C).

The salinity distribution between the coasts of Australia and Antarctica during summer is shown in figure 7. Lower salinity is found south of Australia compared to that of south of Africa and the difference is about 0·2‰ along the same latitude of

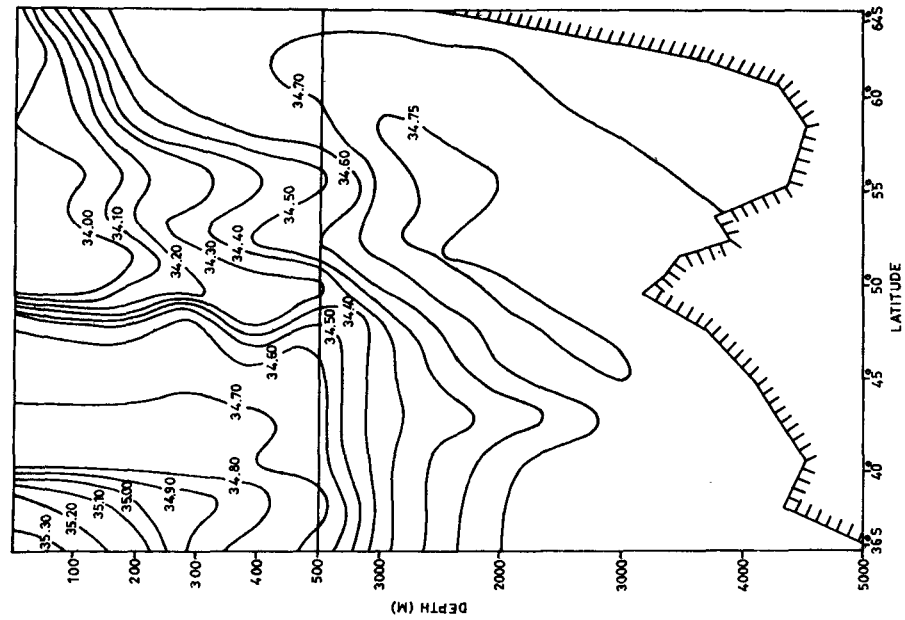

Figure 7. Vertical section of salinity along 115°E.

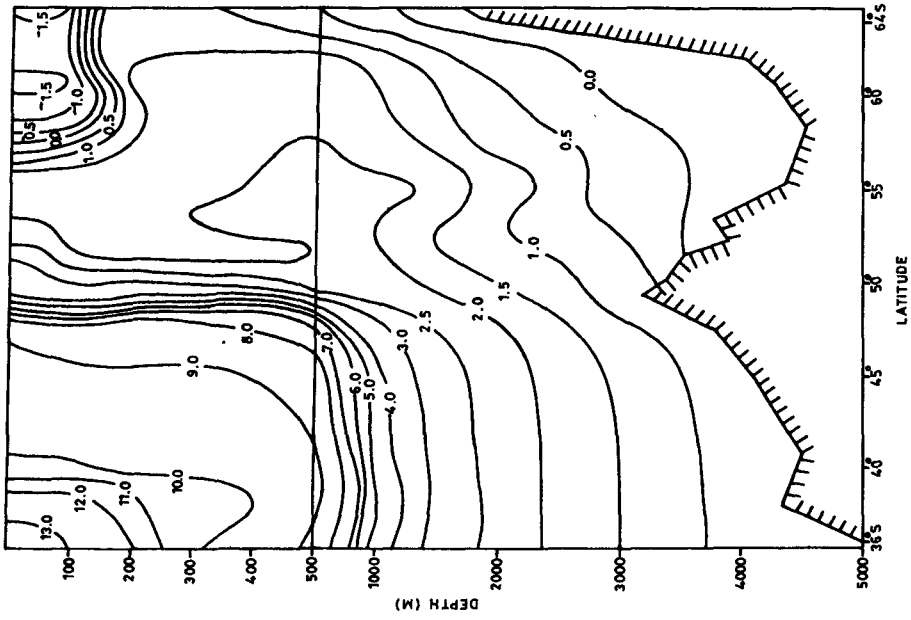

Figure 6. Vertical section of potential temperature along 115°E.

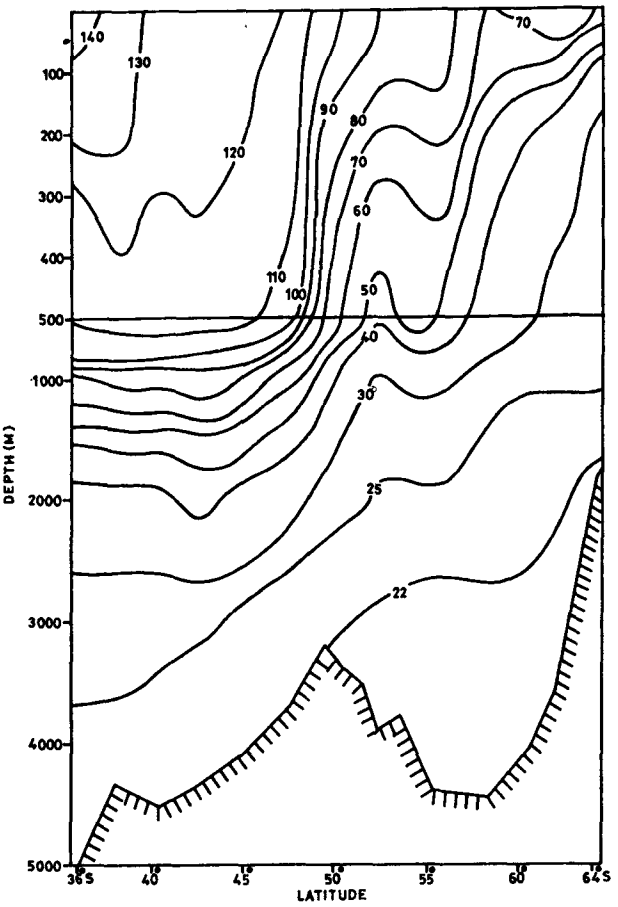

Figure 8. Vertical section of potential thermosteric anomaly along 115°E.

36°S. In the Antarctic zone, a homogeneous surface layer with salinity around 34·0‰ is noticed. The weak halocline, found in the Antarctic zone seems to be surfacing near the Antarctic Continent. Strong variation in salinity noticed at about 47°–48°S identifies the sub-Antarctic front. The subtropical front noticed on this section with strong horizontal gradients, north of 40°S, is not prominent as along 10°E.

Sharp density gradient is noticed at the frontal zones and the sub-Antarctic front is stronger than the Antarctic polar front along 115°E (figure 8). The sloping of isanosteres at the sub-Antarctic Front indicates that maximum flow of the Antarctic circumpolar current occurs in this region.

4. Zonal flux

The zonal mass transport referred to 3000 db along 10°E and 115°E towards east and west is separately calculated and presented to study the latitudinal variation in figures 9 and 10 and its characteristics in figures 11 and 12.

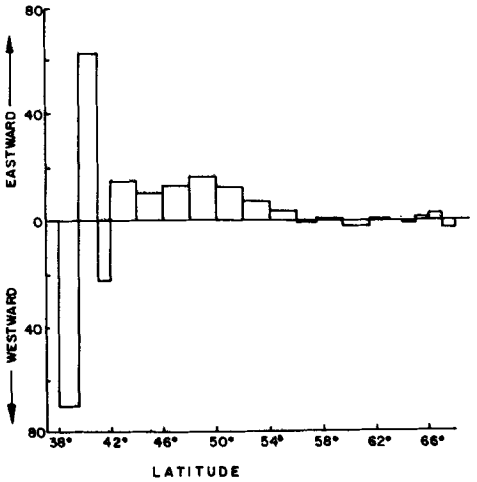

Figure 9. Latitudinal distribution of zonal flux at 10°E.

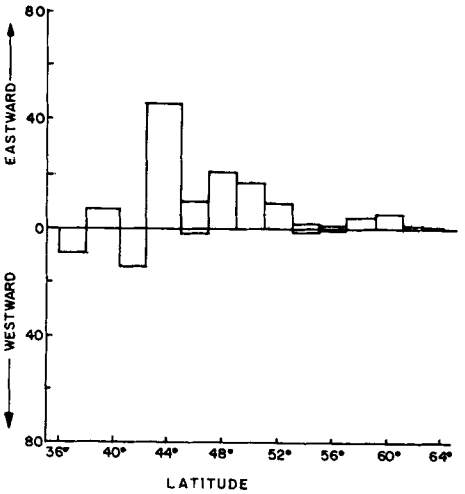

Figure 10. Latitudinal distribution of zonal flux at 115°E.

4.1 *Latitudinal distribution*

The latitudinal distribution of flux along 10°E shows strong westward and eastward flows between 38°S and 41°S which indicates the presence of Agulhas and its return current (Gordon *et al* 1978). The estimated transport of the Agulhas Current across this section is 69·92 Sv and its return flow has a transport of 62·26 Sv. Continuous eastward flow between 42°S and 56°S represents the Antarctic circumpolar current. A maximum transport of the Antarctic circumpolar current is observed between 48°S and 50°S, which seems to be associated with the Antarctic polar front. Weak alternate bands of westerly and easterly flow are observed between 56°S and the Antarctic Coast. Westerly flow associated with the eastwind drift prevails near the coast. Near the Antarctic divergence zone (63°S–64°S), the zonal flux is almost nil. This may be

due to the fact that the transport is mainly vertical at the divergence region. Comparatively strong eastward and westward flows, occurring at the southern end of this section may be part of the Weddell Sea cyclonic Gyre.

The zonal transport during November-December across 115°E (between Australia and Antarctica) is shown in figure 10. The major westward flux is at 41°S while the eastward maximum of 45·29 Sv is observed between 42°S and 45°S. More than 80% of the easterly and westerly fluxes are accounted between 36°S and 53°S. The net flux between 36°S and 42°S is westward, implying the influx of Pacific Ocean Water into the Indian Ocean region.

4.2 *Bivariate distribution of zonal flux*

The bivariate distribution of flux across 10°E is shown in figure 11. The large frequency of fluxes in 50 classes reveals the heterogeneous nature of the transport. The primary mode of eastward and westward fluxes is found around 30 cl/t steric level, having values of 27·27 Sv and 10·83 Sv respectively. Salinity of primary mode is 34·7‰ with a temperature of 1·0°C. Thus, the hydrographic characteristics confer that this mode occurs in the deeper layers.

The secondary mode of easterly flux (11·48 Sv) is observed between 60 and 80 cl/t surfaces in the salinity and temperature ranges of 34·2–34·4‰ and 2°–3°C respectively. The next mode has a flux of 10·11 Sv and is found around 50 cl/t with salinity 34·5‰. Thus, the properties of these modes suggest that the flow is taking place above the primary mode level. The secondary mode of westerly flow is around 90 cl/t while the tertiary is between 140 and 160 cl/t. Evidently these modes are in the surface layers. Thus the secondary and tertiary modes of westerly flow is found at higher steric levels compared to the eastward flow which indicates that the latter is mainly confined to the deeper layers while the westward flow is relatively confined in the upper layers. Within the 50% limit of eastward flow there are eight frequencies whereas the westward flux has seven frequencies. Maximum eastward and westward transports of 41·31 Sv and 23·95 Sv are observed as univariate distribution of salinity 34·7‰. The fairly large flux at salinity exceeding 35·2‰ in the westward direction clearly suggests the remarkable inflow of the subtropical water through the Agulhas Current. The eastward flow is absent above 220 cl/t surface which implies that the surface flow is purely westerly with salinity greater that 35·2‰. The westward flow along upper steric surface (about 5·93 Sv) has high temperature and salinity and is a part of the Agulhas Current.

The bimodal distribution of flux across 115°E (figure 12) between 36°S and 64°S covers 25 characteristic classes between 33·8 and 35·4‰ in salinity and 20 and 160 cl/t in the thermosteric anomaly. The eastward transport is 123·46 Sv whereas the westward flux is 27·20 Sv. The 50% level of easterly flux comprises of four frequencies. The primary and secondary modes are observed in the same salinity intervals of 34·6–34·8‰, but they are at around 30 and 110 cl/t surfaces respectively. The primary mode of easterly flux has the value of 32·75 Sv while the secondary has only 12·19 Sv. The next two frequencies within the 50% level of easterly flow have fluxes of 11·36 Sv and 9·05 Sv. The physical properties confirm that the primary mode is in the deeper layer and other modes occur above it. The primary mode of westerly flux coincides with the secondary mode of the easterly flux and has transport of 4·49 Sv. Thus, the primary mode of westerly flux occurs in the upper layers. The other three frequencies within the 50% level of the westerly flux are below 80 cl/t steric level.

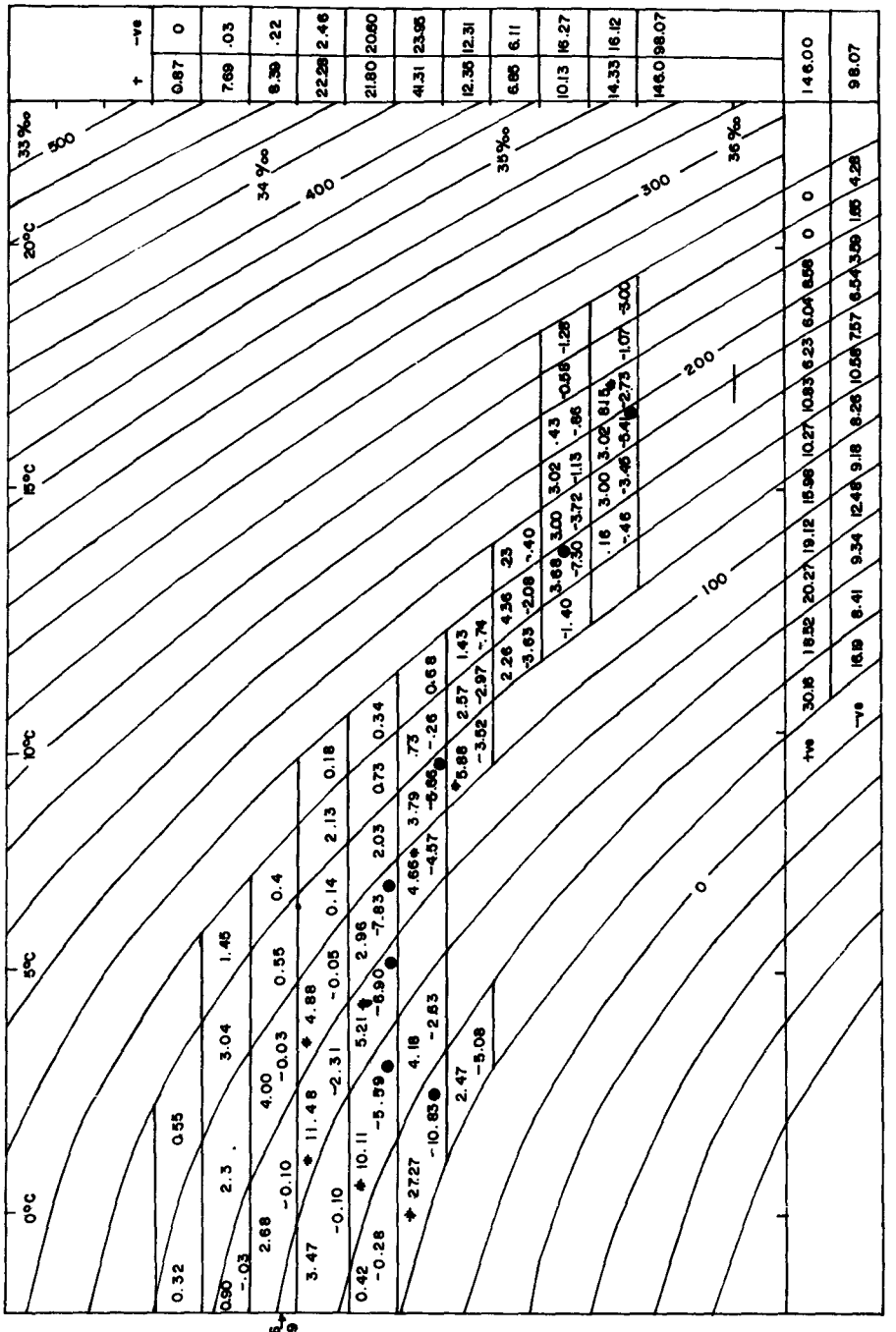

Figure 11. Bivariate distribution of zonal flux at 10°E.

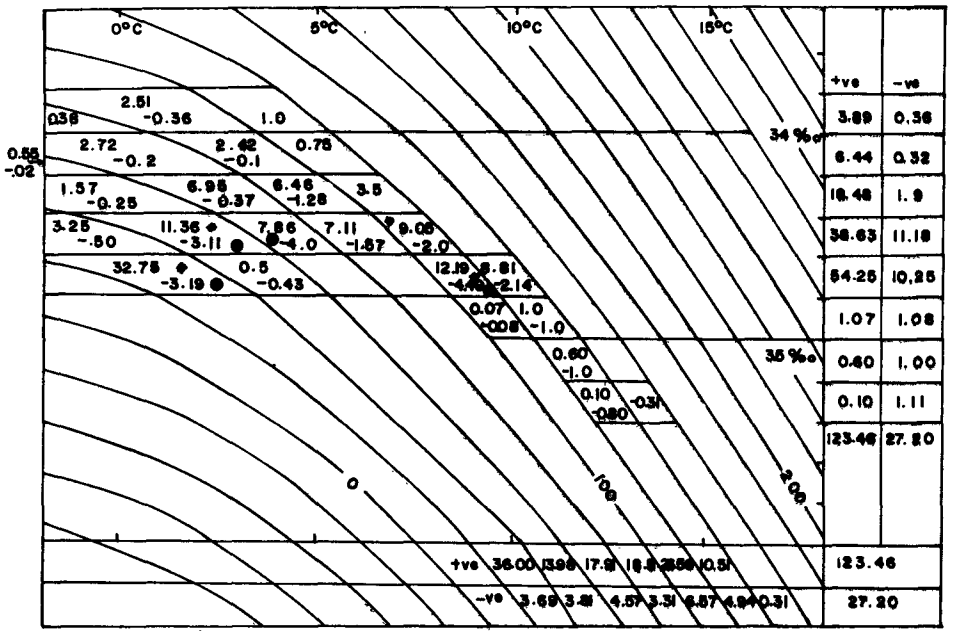

Figure 12. Bivariate distribution of zonal flux at 115°E.

With respect to the salinity, the maximum eastward flux is at 34·7‰ whereas the westward flux is around 34·5‰. More uniformity of the flux with respect to the steric surfaces than to the salinity shows the dominant influence of salinity in the transport. Maximum negative transport is observed at a higher steric level of 100–120 cl/t whereas the eastward maximum is in the 20–40 cl/t class.

5. Discussion

A comparison of the estimated flux shows a general agreement with the previous estimations. Jacobs and Georgi (1977) estimated an eastward transport 129 Sv between Africa and Antarctica, whereas George and Toole (1982) computed the volume transport south of Africa as 140 Sv.

The zonal flux distribution across 10°E during December-January clearly represents the intense Agulhas Current flowing southwestward along the African Coast. Nearly 70% of the westward flux along 10°E is contributed by the Agulhas Current itself. The estimated transport of 69·92 Sv for the Agulhas Current is in agreement with the earlier computations of Grundlingh (1980). This current feeds the Agulhas return flow near 40°S introducing large quantities of warm saline water south of Africa resulting in a large heat flux to the atmosphere. Grundlingh (1978) identified the rapid eastward return of the Agulhas current west of 20°E and its path towards the east along 40°S. The transport estimates clearly reveal westward flux between 50°S and 60°S in the section at 10°E. This westward transport corresponds to the Weddell Gyre described by Koopman (1953), Mackintosh (1972) and Deacon (1979). It is interesting to note that a major portion of the flux occurs at subsurface levels, though the westward

transport associated with the Weddell Gyre is small. This is in consistency with the results of Deacon (1979). The westward flow associated with the eastward drift near the Antarctic Coast is evident in the western side at 10°E.

The mass transport, obtained at the eastern boundary at 115°E is in consensus with the results of Gordon (1975), Georgi and Toole (1982) and their values of volume transport are 135 Sv and 125 Sv respectively for a north-south section, south of New Zealand. Callahan (1971) calculated the transport between Australia and Antarctica and his values slightly exceed the present ones, probably due to the change in reference level. The westward flowing Australian Coastal Current is very clear in the Section at 115°E.

Comparison of fluxes at 10°E and 115°E shows that the net transport from the Atlantic to Indian Ocean is 47·93 Sv while the net flow from the Indian to Pacific Ocean is about 96·26 Sv. The Indian Ocean thus has a net loss of 48·33 Sv. This loss must have been balanced by melting of ice and influx of equatorial Pacific Ocean water. Between Asia and Australia there is an influx of Pacific Water carried by the south equatorial current (Wyrtki 1961; Sharma *et al* 1978). Godfrey and Golding (1981) conclude that the mean volume flux from Pacific to Indian Ocean could be about 10Sv, though marked deviations from the mean can occur.

Bimodal representation of the zonal flux shows that the Antarctic circumpolar current is more homogeneous in the east. The heterogeneity south of Africa is due to addition of highly saline and warm subtropical waters carried by the Agulhas Current and the intrusion of cold low saline Weddell Sea Water from the south. It is also noted that the warmest and saltiest water of the Southern Ocean are found south of Africa. The characteristics of the computed fluxes suggest that there is a net transport to the Pacific Ocean in the surface layers. This confirms that an increased production of surface waters in the south also contributes to the excess flow to the Pacific Ocean.

The primary mode characteristics confirm the major contribution of circumpolar deep water to the Antarctic circumpolar current. The flux distribution with respect to the different steric surfaces indicates that the maximum fluxes are taking in subsurface levels.

6. Conclusions

Considering the inter-oceanic exchanges between Atlantic, Indian and Pacific oceans it is found that the Indian Ocean is losing an additional 48·33 Sv into the Pacific Ocean than what it gains from the Atlantic Ocean. This intrusion of equatorial Pacific Ocean water north of Australia also contributes to balance the outflow from the Indian Ocean.

The bimodal representation of transport indicates that a major part of the excess outflow to the Pacific Ocean occurs in the surface layers, i.e., along the Antarctic surface water. The higher production of ice melt water in the south probably compensates part of the net loss to the Pacific Ocean.

The distribution of zonal flux denotes that a major part of the flow takes place in the subsurface levels, compared to the surface layers. The characteristics of the flow shows that the major part of the circumpolar current is constituted by the circumpolar deep water. In general, the flux is found to be more homogeneous in the eastern side compared to the west.

The latitudinal distribution of zonal flux reveals the multistream structure of the Antarctic circumpolar current. It is embedded with several strong and weak flows. The maximum flow occurring at the Polar front region implies the importance of thermohaline driving of the Antarctic circumpolar current.

Acknowledgements

The results of this paper were presented in the IAPSO Section of the XIX IUGG General Assembly held at Vancouver, Canada during 9–22 August, 1987. One of the authors (BNP) is grateful to CSIR, New Delhi for financial assistance.

References

Bryden H L and Pillsbury R D 1977 Variability of deep flow in the Drake passage from year-long current measurements; *J. Phys. Oceanogr.* **7** 803–810

Callahan J E 1971 Velocity structure and flux of the Antarctic Circumpolar Current South of Australia; *J. Geophys. Res.* **76** 5859–5864

Deacon G E R 1979 The Weddell Gyre; *Deep Sea Res.* **26** 981–995

Fandry C and Pillsbury R D 1979 On the estimation of absolute geostrophic volume transport applied to the Antarctic circumpolar current; *J. Phys. Oceanogr.* **9** 499–555

Georgi D T and Toole J M 1982 Antarctic circumpolar current and oceanic heat and freshwater budgets; *J. Mar. Res.* **40** 183–197

Godfrey J S and Golding T J 1981 The Sverdrup relation in the Indian Ocean, and the effect of Pacific-Indian through flow on Indian Ocean circulation and on the East Australian Current; *J. Phys. Oceanogr.* **11** 771–779

Gordon A L 1975 An Antarctic oceanographic section along 170°E; *Deep Sea Res.* **22** 357–377

Gordon A L, Molinelli E J and Baker T N 1978 Large scale relative dynamic topography of the Southern Ocean; *J. Geophys. Res.* **83** 3023–3032

Grundlingh M L 1978 Drift of a sateliite-tracked buoy in the southern Agulhas current and Agulhas return current; *Deep Sea Res.* **25** 1209–1224

Grundlingh M L 1980 On the volume transport of the Agulhas Current; *Deep Sea Res.* **27** 557–563

Jacobs S S and Georgi D T 1977 Observations on the southwest Indian/Antarctic Ocean; *In a voyage of discovery* (ed) M. Angel (Oxford: Pergamon Press) pp 43–84

Koopmann G 1953 Ebtstehung Und Verbrietung Von Divergenzen in der obevflaschennahen Wasserbemegung der antarkischen; *Dtsch. Hydrogr. Z. Ergaenzungsh.* **2** 38 pp + 2 plates

Kort V G 1962 The Antarctic Ocean; *Sci. Am.* **207** 113–128

Mackintosh N A 1972 Life cycle of Antarctic Krill in relation to ice and water conditions; *Discovery Rep.* **36** 1–94

Montgomery R B and Spilhaus A F 1941 Examples and outline of certain modification in upper air analysis; *J. Aero. Sci.* **8** 276–283

Montgomery R B and Stroup E D 1962 Equatorial waters and currents at 150°W in July–Aug. 1952; *John Hopkins Oceanogr.* **1** 68 pp

Nowlin W D Whitworth T III and Pillsbury R D 1977 Structure and transport of Antarctic circumpolar current at Drake passage from short-term measurements; *J. Phys. Oceanogr.* **7** 788–802

Reid J L and Nowlin W D Jr 1971 Transport of Water through the Drake Passage; *Deep. Sea Res.* **18** 51–64

Sharma G S, Gouvia A D and Shubha Sathyendranath 1978 Incursion of the Pacific Ocean Water into the Indian Ocean; *Proc. Indian Acad. Sci. (Earth Planet. Sci.)* **87** 29–45

Sverdrup H U, Johnson M V and Fleming R H 1942 *The Oceans* (Englewood Cliffs, NJ, USA; Prentice-Hall) pp. 1087

Wyrtki K 1961 Scientific results of marine investigations of the South China Sea and the Gulf of Thailand, Physical oceanography of the southeast Asian Waters; NAGA Report 2. 195 pp